

1
2
3
4
5
6
7
8
9
10
11
12
13
14
15
16
17
18
19
20
21
22
23
24
25
26
27
28
29

Revision 1 – 06/26/2013

Monipite, MoNiP, a new phosphide mineral in a Ca-Al-rich inclusion from the Allende meteorite

Chi Ma*, John R. Beckett, George R. Rossman
Division of Geological and Planetary Sciences
California Institute of Technology
Pasadena, CA 91125, USA

ABSTRACT

Monipite (IMA 2007-033), MoNiP, is a new phosphide mineral that occurs as one $1 \times 2 \mu\text{m}$ crystal in a Type B1 Ca-Al-rich inclusion (CAI) ACM-2 from the Allende CV3 carbonaceous chondrite. It has a $P\bar{6}2m$ Fe₂P type structure with $a = 5.861 \text{ \AA}$, $c = 3.704 \text{ \AA}$, $V = 110.19 \text{ \AA}^3$, and $Z = 3$. The calculated density using our measured composition is 8.27 g/cm^3 , making monipite the densest known mineral phosphide. Monipite probably either crystallized from an immiscible P-rich melt that had exsolved from an Fe-Ni-enriched alloy melt that formed during melting of the host CAI or it exsolved from a solidified alloy. Most of the original phosphide in the type occurrence was later altered to apatite and Mo-oxides, leaving only a small residual grain. Monipite occurs within an opaque assemblage included in melilite that contains kamiokite (Fe₂Mo₃O₈), tugarinovite (MoO₂), and a Nb-rich oxide ((Nb,V,Fe)O₂), none of which has previously been reported in meteorites, together with apatite, Ni₂Fe metal, and vanadian magnetite.

Keywords: monipite, MoNiP, new mineral, tugarinovite, kamiokite, Allende, carbonaceous chondrites, EBSD, Ca-, Al-rich inclusions

*E-mail: chi@gps.caltech.edu

30

INTRODUCTION

31 Schreibersite and barringerite are well known phosphides from iron and stony iron
32 meteorites but phosphides are rare in carbonaceous chondrites, very rare in CV3 chondrites
33 (Jambor et al. 2000; Riches et al. 2010) and, to our knowledge, have not been reported at all
34 in Allende. It is phosphates, not phosphides, that are typically observed in carbonaceous
35 chondrites (e.g., Armstrong et al. 1985, 1987). The reason for this is straightforward.
36 Conditions during metasomatism of Allende and similar meteorites were quite oxidizing
37 such that phosphates became the stable P-bearing minerals. Exposed phosphides were
38 generally destroyed but, here, we describe monipite, a rare phosphide survivor of the
39 metasomatism of the Allende CV3 carbonaceous chondrite, and explore its origin and
40 evolution. Preliminary results are given in Ma et al. (2009a).

41 The ternary phosphide MoNiP is a well-known synthetic material because of its
42 potential use as a hydrodesulfurization catalyst during petroleum refining (e.g., Sun et al.
43 2004; Nagai et al. 2005) and because it is a superconductor with a high, for a phosphide,
44 critical temperature (Shirovani et al. 2000). Monipite, natural MoNiP, is the first phosphide
45 mineral with molybdenum as a major constituent and the second mineral with the
46 barringerite Fe₂P type structure. It is also the first reported occurrence of a phosphide in
47 Allende.

48

49

MINERAL NAME AND TYPE MATERIAL

50 The new mineral and its name have been approved by the Commission on New
51 Minerals, Nomenclature and Classification of the International Mineralogical Association
52 (IMA 2007-033). Monipite is the Mo-, Ni-dominant analog of barringerite, Fe₂P. The
53 mineral name monipite is derived from the three major elemental constituents
54 (**M**olybdenum, **N**ickel, and **P**hosphorus). A polished thin section, prepared from a 1-cm-
55 diameter Allende fragment (Caltech Meteorite Collection No. Allende-12A) contains the
56 holotype material of monipite within a CAI. This section was deposited in the Smithsonian
57 Institution's National Museum of Natural History with the catalog number USNM 7554.
58 Type allendeite, grossmanite, hexamolybdenum and hibonite-(Fe), which were described by
59 Ma and Rossman (2009b), Ma et al. (2009b) and Ma (2010), are also present in this section.

60

61 **APPEARANCE, PHYSICAL, AND OPTICAL PROPERTIES**

62 The holotype grain of monipite is $1 \times 2 \mu\text{m}$ in the plane of the section (Fig. 2; see Fig. 1
63 for a larger scale petrographic context). It is in contact with apatite, tugarinovite (MoO_2), and a
64 Ru-Mo-Ni enriched alloy. The grain is opaque and non-cathodoluminescent under the electron
65 beam in an SEM. Luster, streak, hardness, cleavage, fracture, and details of the optical
66 properties were not determined because of the small grain size. The calculated density using our
67 measured composition and the structure and cell parameters of synthetic MoNiP from Guérin and
68 Sergent (1977) is 8.27 g/cm^3 (see below).

69

70 **CHEMICAL COMPOSITION**

71 Backscatter electron (BSE) images were obtained using a ZEISS 1550VP field emission
72 SEM and a JEOL 8200 electron microprobe with solid-state BSE detectors. Quantitative
73 elemental micro-analyses were conducted with the JEOL 8200 electron microprobe operated at
74 15 kV and 5 nA in focused beam mode. Standards for the analysis of monipite were Mo ($\text{MoL}\alpha$),
75 Ni ($\text{NiK}\alpha$), GaP ($\text{PK}\alpha$), Ru ($\text{RuL}\alpha$), Rh ($\text{RhL}\alpha$), Fe ($\text{FeK}\alpha$), and Co ($\text{CoK}\alpha$). Analyses were
76 processed using the CITZAF correction procedure (Armstrong 1995). An Oxford INCA X-ray
77 energy dispersive spectrometer (EDS) on the ZEISS SEM was also used for elemental analysis.
78 These data were processed using the XPP correction procedure (Pouchou and Pichoir 1991).

79 Compositions of phases from the host inclusion, oxides and apatite from the opaque
80 assemblage containing monipite are given in Table 1. In Table 2 we give compositions of alloys
81 and monipite. Opaque assemblages are complex, multi-phase objects that occur in carbonaceous
82 chondrites [see Blum et al. (1989) for a general description] and are generally thought to be
83 oxidation/sulfidation products of alloys or alloy-rich phase assemblages. Some of the
84 compositions reported in Table 1 reflect mixtures of the target phase with nearby or surrounding
85 phases. Such data are the best we can do at present and are given to maximize information about
86 the phase assemblages in the vicinity of monipite.

87

88 **CRYSTALLOGRAPHY**

89 Single-crystal electron backscatter diffraction (EBSD) analyses at a sub-micrometer scale
90 were performed using an HKL EBSD system on the ZEISS 1550VP scanning electron
91 microscope operated at 20 kV and 9 nA in focused beam mode with a 70° tilted stage and in a

92 variable pressure mode (25 Pa). The EBSD system was calibrated using a single-crystal silicon
93 standard. The structure of monipite was determined and cell constants obtained by matching the
94 observed EBSD pattern against the structures of synthetic phases in the Mo-Ni-P system (Guérin
95 and Sergent 1977; Shirotani et al. 2000). The $P\bar{6}2m$ MoNiP structure (Guérin and Sergent 1977)
96 yields the lowest mean angular deviation (MAD) with MAD values of $0.3^\circ \sim 0.7^\circ$ (Fig. 3).
97 Alternative candidate structures had much higher MAD values ($\sim 1.0^\circ$).

98 From the cell parameters of MoNiP (Guérin and Sergent 1977), the cell parameters for
99 monipite are $a = 5.861 \text{ \AA}$, $c = 3.704 \text{ \AA}$, $V = 110.19 \text{ \AA}^3$, $Z = 3$. Note that errors are not given for
100 these cell parameters because they are taken directly from the data of the matching synthetic
101 phase. Accepting these parameters for monipite, the calculated density using our measured
102 composition is then 8.27 g/cm^3 , which is the highest known density for a natural phosphide.
103 Monipite assumes a Fe_2P type structure constructed from successive layers of Ni + P and Mo + P
104 with Ni and Mo in tetrahedral and square-pyramidal coordination, respectively (Guérin and
105 Sergent 1977; Shirotani et al. 2000).

106 The X-ray powder-diffraction data (in Å for $\text{CuK}\alpha 1$) are taken from PDF 71-0202. The
107 strongest calculated lines are [d in Å , intensity, I, scaled to 100 for the most intense peak, (hkl)]
108 [2.298, 100, (111)], [1.918, 73, (210)], [2.094, 69, (201)], [1.852, 24, (002)], [1.408, 20, (310)],
109 [1.316, 18, (311)], [1.332, 17, (212)], and [1.111, 14, (321)].

110 Raman micro-analysis of monipite was carried out using a Renishaw M1000 micro-
111 Raman spectrometer system and a 514.5 nm laser using methods described in Ma and Rossman
112 (2008, 2009a). The Raman spectrum for monipite (Fig. 4), shows Raman features at 280, 350,
113 and 430 cm^{-1} .

114

115 OCCURRENCE AND ASSOCIATED MINERALS

116 Monipite occurs as one irregular grain, $1.3 \times 2.0 \text{ }\mu\text{m}$ in size (Figs. 1 - 2), in the central
117 portion of an opaque assemblage (Blum et al. 1989) enclosed mostly within melilite from a
118 fragment of a coarse-grained Ca-, Al-rich inclusion, ACM-2. There are also some coarse spinel
119 grains in contact with the opaque assemblage. The monipite is approximately $1100 \text{ }\mu\text{m}$ from the
120 surface of the inclusion as defined by a Wark-Lovering rim in the plane of the section, which
121 consists of a series of mono- and bi-mineralic layers, abutting matrix; these rims surround most
122 coarse-grained inclusions in Allende (Fig. 1a; see Wark and Boynton 2001 and references

123 therein). Since the Wark-Lovering rim is absent on the side closest to the monipite, we can
124 conclude that only a portion of the original inclusion has survived. The distance to the opposite,
125 now missing, free surface, which would also have been bounded by a Wark-Lovering rim, is
126 unknown but we argue below that the Wark-Lovering rim shown in Fig. 1a marks the free
127 surface closest to the monipite. The surviving portion of the host inclusion is $\sim 1400 \times 2800 \mu\text{m}$
128 across in the plane of the type section (Fig. 1a). The observed host inclusion is melilite-rich (>90
129 % modal melilite) with minor amounts of clinopyroxene (a solid solution between Al,Ti-diopside
130 and grossmanite) and MgAl_2O_4 spinel, most of the latter residing in a band $\sim 200 \mu\text{m}$ inboard
131 from the Wark-Lovering rim. These features are potentially consistent with either a compact type
132 A (CTA) inclusion, in which the mode is everywhere dominated by melilite with minor spinel
133 and clinopyroxene, or the melilite-rich mantle portion of a type B1 inclusion. In type B1
134 inclusions, the melilite-rich mantle surrounds a core containing major modal clinopyroxene
135 along with melilite, spinel, and, usually, anorthite. Since these inclusion types have
136 significantly different bulk compositions and may have had significantly different histories (e.g.,
137 Grossman et al. 2008a), it is desirable to distinguish between these two possibilities. We,
138 therefore, begin with a consideration of the host inclusion and its petrographic type and then
139 describe the immediate environs of the type monipite grain.

140 Based on multiple sections cut through the inclusion of this study, the plane of the thin
141 section is roughly perpendicular of the surface of the original inclusion and, assuming that the
142 inclusion was originally spherical, we estimate that it was roughly 7 mm in diameter (estimated
143 via Figure 1a for a chord $1380 \mu\text{m}$ across with a segment height of $260 \mu\text{m}$). Such a large CAI
144 would be consistent with a type B1 inclusion but unusual for CTA inclusions, which tend to be
145 much smaller, although TS12, a CTA described by Simon et al. (1999), is 8 mm long \times 1.5 mm
146 across in section. Although a CTA is possible based on observed dimensions of the inclusion
147 fragment sampled by USNM 7554, it is much more likely that *ACM-2* is a type B1 inclusion.

148 The major element chemistries of melilite and spinel in *ACM-2* are not diagnostic for
149 inclusion type. Highly magnesian melilites in a melilite-rich CAI would be a signature for a type
150 B1 inclusion but the relatively aluminous melilites observed in *ACM-2* are consistent with both
151 type B1 and CTA inclusions. The composition of clinopyroxene, however, does provide an
152 additional clue to the identity of the host inclusion. Clinopyroxene occurring near the Wark-
153 Lovering rim is highly titaniferous with TiO_2^* (all Ti calculated as TiO_2) as high as 19 wt %.

154 The type grossmanite crystal, which was described by Ma and Rossman (2009b), also occurs in
155 USNM 7554 and its location is indicated in Fig. 1. Grossmanites are not diagnostic for inclusion
156 type because they found in both CTAs and in the melilite-rich mantles of type B1 inclusions.
157 However, clinopyroxene in the vicinity of the monipite-bearing opaque assemblage is Al,Ti-
158 diopside, characterized by relatively modest TiO_2^* contents (e.g., Table 1) ranging from 6 - 9 wt
159 %. This strongly suggests that the host inclusion is a type B1 (Simon et al. 1999). It seems
160 likely that the original inclusion broke at or near the interface between the mantle and core, a
161 natural zone of weakness, and that the monipite-bearing section shown in Fig. 1 is part of a
162 fragment that adhered to the matrix after removal of the bulk of the inclusion.

163 The monipite crystal (Fig. 2) is in contact with a Ru-Mo-Ni metal grain
164 ($\text{Ru}_{0.47}\text{Mo}_{0.28}\text{Ni}_{0.22}\text{Rh}_{0.04}$), which has a $\text{P6}_3/\text{mmc}$ structure based on EBSD measurements, apatite
165 (identity confirmed via EBSD versus merrillite), and tugarinovite (MoO_2), which also occurs
166 partially included in the Ru-enriched alloy. An Nb-rich oxide (Nb,V,Fe) O_2 , an unnamed cubic
167 Mo-Fe oxide, V-Mo-bearing magnetite, kamiokite, spinel, tugarinovite, and awaruite are also
168 present elsewhere in the opaque assemblage; compositions obtained via SEM-EDS or EPMA are
169 given in Tables 1-2. The Nb-rich oxide has, after extracting P_2O_5 and CaO in the form of apatite
170 a formula of $(\text{Nb}_{0.54}\text{V}_{0.27}\text{Fe}_{0.15}\text{Mg}_{0.05}\text{Al}_{0.04})\text{O}_2$. This phase is different from the one described by
171 Lovering et al. (1979). Their grains have much higher molar Ca/Nb (~1) and are likely to be
172 pyrochlores, as suggested by the authors.

173 The monipite-Ru-Mo-Ni alloy- tugarinovite assemblage is surrounded by apatite and an
174 asymmetric suite of partial bi- to polymineralic rings with the Nb-rich oxide
175 $(\text{Nb}_{0.54}\text{V}_{0.27}\text{Fe}_{0.15}\text{Mg}_{0.05}\text{Al}_{0.04})\text{O}_2$ restricted to the pyroxene-spinel bounded side of the opaque
176 assemblage and Mo-Fe oxides generally restricted to the awaruite side in Fig. 2. Apatite
177 (identity confirmed via EBSD) is found throughout the opaque assemblage in Fig. 2 up to the
178 interface with the large Ni_2Fe grain but no Ru enriched alloys are observed in this region,
179 although they do occur as submicron inclusions included in the large Ni_2Fe grain. Tugarinovite
180 gives way to one or more Mo-Fe oxides with an overall molar Mo/Fe ~ 2, at least one of which is
181 cubic (i.e., not tugarinovite or kamiokite), and kamiokite ($\text{Fe}_2^+\text{Mo}_3^{4+}\text{O}_8$). Continuing left in Fig.
182 2, these phases are largely replaced by a Mo-, V-rich magnetite. A grain of kamiokite is,
183 however, observed at the edge of the large Ni_2Fe metal grain shown in Figs. 1b and 2 and both
184 kamiokite and Ru-Os-Mo enriched alloy grains occur as inclusions within it. Sprays of V-rich

185 magnetite and Ni₂Fe metal extend outward from the monipite-bearing assemblage along cracks
186 (Fig. 1b), suggesting mobility of Fe, Ni, and V.

187 We did not observe any additional monipite-bearing phase assemblages in ten sections
188 taken in series through the CAI shown in Figs. 1-2. Molybdenite (MoS₂) is observed in one
189 opaque assemblage with pentlandite and Pt-Ir enriched Ni-Fe alloy (Ni₅₀Fe₃₀Pt₁₇Ir₃) but Mo is
190 more typically found in the form of oxides. Kamiokite is observed as inclusions in two Ni-Fe
191 alloys; for these grains, no associated opaque assemblages were observed, although one of them
192 had a phosphate in contact with the Ni-Fe alloy. We also encountered two opaque assemblages
193 containing both phosphate and Mo oxides (Fig. 5). In one of these (Fig. 5a), a mixture of apatite
194 and Mo-Fe oxide / tugarinovite forms a patch partially intruding a large grain of Ni-Fe alloy.
195 The other example (Fig. 5b) contains a rounded cluster of tugarinovite and apatite bounded by
196 kamiokite and a Pt-enriched Fe-Ni alloy.

197 Phase compositions are given in Tables 1-2. From EPMA, the monipite crystal has an
198 empirical formula of (Mo_{0.84} Fe_{0.06} Co_{0.04} Rh_{0.03})_{Σ0.97} (Ni_{0.89} Ru_{0.09})_{Σ0.98} P. Spinel is Mg-, Al-rich
199 but generally zoned in Fe with iron decreasing from rim to core. Clinopyroxene compositions
200 are discussed above. Chlorine and F were not detected in apatite using SEM-EDS but we did not
201 attempt to quantify halogen concentrations using EPMA. Apatite in an opaque assemblage from
202 an Allende CAI described by Armstrong et al. (1985) contained 1.6 wt.% Cl so it is possible that
203 the apatite shown in Figs. 1-2 also contains significant concentrations of Cl. To our knowledge,
204 monipite is the first known occurrence of a phosphide in Allende, although phosphides have
205 been reported in other CV3 chondrites such as Efremovka (Jambor et al. 2000) and NWA 6101
206 (Riches et al. 2010).

207

208

ORIGIN AND SIGNIFICANCE

209 Monipite joins allabogdanite (Fe,Ni)₂P, andreiyvanovite (FeCrP), barringerite (Fe₂P), and
210 florenskyite (FeTiP), as the minerals with an M₂P stoichiometry, where “M” represents a cation.
211 Other phosphide minerals (e.g., schreibersite) have an M₃P or M₄P stoichiometry. Monipite is
212 also the only phosphide mineral with Mo as a major component. This is also the first reported
213 meteoritic occurrence of kamiokite and tugarinovite (and of the unnamed Nb-V and Mo-Fe
214 oxides) in a meteorite. In this section, we briefly consider constraints on the origin of monipite.
215 We begin with a consideration of monipite stability and general thermal history constraints

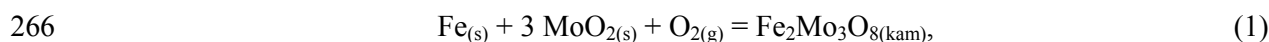
216 derived from Type B1 inclusions, then sort out the signatures from low temperature metasomatic
217 processes and, finally, place monipite within the overall history of the CAI.

218 Monipite is readily synthesized on composition in sealed silica tubes between 800 and
219 1200°C (Guérin and Sargent 1977; Oryshchyn et al. 2001) and at high pressure (Shirotni et al.
220 2000) but neither high nor low temperature stability limits have been established. MoNiP is also
221 known to precipitate readily in arc melted, very rapidly cooled, Pd-Ni-Cu-P glassy alloys, even
222 at small concentrations of Mo (≤ 3 wt. %; Ma and Inoue 2003), suggesting that MoNiP may be
223 stable to the high temperatures encountered during melting of the host CAI. Thermodynamic
224 and relevant high temperature phase equilibria data are, however, lacking for monipite, so we
225 cannot use them for a quantitative evaluation of the stability of this phase.

226 The high temperature history of the host CAI would normally provide the basic
227 framework for discussing the origin of monipite but most of the CAI is missing and we must,
228 therefore, resort to, generic constraints based on other Allende type B1 inclusions. A variety of
229 textural and compositional constraints (Stolper 1982; Stolper and Paque 1986; Grossman et al.
230 2008b) imply maximum temperatures for type B1 inclusions of roughly 1400-1450°C with
231 subsequent cooling at rates of degrees to tens of degrees °C/hr under highly reducing conditions.
232 Brief excursions to higher temperatures are possible but both petrographic and isotopic
233 constraints argue against any extended residence (Stolper and Paque 1986; Richter et al. 2002).
234 For Type B1 inclusions, formation of the melilite-rich mantle appears to have been a
235 consequence of the volatilization of Mg and Si from near surface regions of the partially molten
236 droplet followed by nucleation and growth of melilite in the Mg-, Si-depleted region (e.g.,
237 Mendybaev et al. 2006). Precursors to the monipite-bearing assemblage shown in Figs. 1-2 and
238 5 and of other assemblages in this CAI now containing the Mo-rich phases tugarinovite and
239 kamiokite were engulfed by melilite when the mantle crystallized. Given the highly reducing
240 conditions during melting of the host CAI (e.g., Stolper et al. 1982; Grossman et al. 2008b), far
241 more reducing than the Mo-MoO₂ buffer, all Mo would have been in reduced form, either in a
242 liquid/crystalline alloy or as a phosphide (i.e., tugarinovite, kamiokite, and apatite are secondary
243 phases). At the ~1400°C peak temperatures of the host CAI, Fe-Ni alloys are crystalline but
244 small amounts of C, P, or S can greatly decrease the liquidus temperature (e.g., Vogel and
245 Horstmann 1953; Gabriel et al. 1987; Waldner and Pelton 2004). The rounded shape of most
246 opaque assemblages in Type B inclusions suggests either brief excursions to temperatures above

247 ~1450°C or the inclusion of small amounts of C, P, and/or S. The monipite-bearing assemblage
248 (Figs. 1-2) and similar opaque assemblage observed in another section through the CAI (Fig. 5)
249 both embay adjacent Fe-Ni alloy and are partially surrounded by spinel and Al,Ti-diopside.
250 These objects differ from typical opaque assemblages in Allende CAIs in containing
251 anomalously large amounts of Mo, which also decreases liquidus temperatures for Fe-Ni-rich
252 compositions and, most importantly, P.

253 Allende CAIs have been altered through oxidation and vapor transport and it is important
254 to evaluate how these secondary processes may have affected monipite and nearby phases. We
255 take the temperature - fO_2 conditions for Ni₂Fe alloy-magnetite equilibrium from McMahon and
256 Haggerty (1980; $\log fO_2 = 8.855 - 28557/T(K)$) and temperatures in the range of 500-800°C as
257 representative of this event (Armstrong et al. 1987; Blum et al. 1989). The Mo-MoO₂ buffer
258 (O'Neill 1986) is approximately two *log* units more reducing than the McMahon-Haggerty
259 conditions, so that tugarinovite (MoO₂) is the stable Mo-O phase during the alteration event, but
260 it is several orders of magnitude more oxidizing than fO_2 s associated with the CAI melting event,
261 so tugarinovite, even had it existed in a precursor, would not have survived the melting event.
262 Tugarinovite is a secondary phase. Similar arguments can be used to assert that kamiokite is also
263 secondary. Large chemical potential gradients are implied by the observed phase assemblages.
264 For example, the activity of MoO₂ is ~1 where tugarinovite is present but only 5 μm away,
265 kamiokite contacts Ni₂Fe, for which the equilibrium can be expressed as



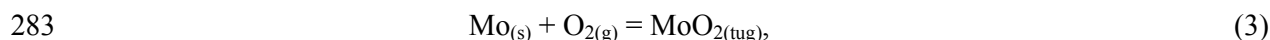
267 where "kam" refers to kamiokite. Writing an equilibrium constant expression for this reaction
268 and solving for the activity of MoO₂ leads to

$$269 \quad a_{MoO_2} = \exp \left\{ \left[\frac{G_{\rightarrow(1)}}{RT} - \ln a_{Fe}^2 - \ln f_{O_2} \right] / 3 \right\}. \quad (2)$$

270 Again, using McMahon and Haggerty to determine temperature - fO_2 with standard state data for
271 Fe-Mo oxides from Chase et al. (1985) and Koyama et al. (2003), and activities of Fe in Fe-Ni
272 solutions (Chuang et al. 1986), we obtain a_{MoO_2} of 0.07 (500°C) to 0.18 (800°C). The opaque
273 assemblage shown in Fig. 2 sustained large gradients in MoO₂ activities over just 5 μm with
274 activities decreasing outward from the center.

275 The Ru_{0.47}Mo_{0.28}Ni_{0.22}Rh_{0.04} alloy adjacent to monipite in Figs. 1b and 2 has a P6₃/mmc
276 structure, which is the same as the element Ru, suggesting that this is a terminal Ru-rich alloy. If

277 so, this is probably a high temperature phase, because Ni solubility in Ru-Ni alloys is less than
278 10 mole% for temperatures below 900°C, although it is possible that Mo stabilizes Ni in Ru-rich
279 solutions. Available thermodynamic data on terminal Ru-rich alloys in the Ru-Ni and Ru-Mo
280 binaries (Kleykamp 1989; Mazhuga et al. 1998) indicate substantial negative deviations from
281 ideality. If the alloy equilibrated to low temperatures with contacting tugarinovite, we can write
282 the formation reaction



284 where "s" refers to the solid Ru-Mo-Ni alloy, "g" to gas, and "tug" to tugarinovite and a
285 corresponding equilibrium constant expression, which can be rearranged to solve for the activity
286 of Mo in the alloy:

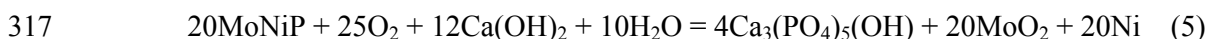
$$287 \quad a_{\text{Mo}} = \exp \left[\frac{G_{\rightarrow(3)}^{\circ}}{RT} - \ln f_{\text{O}_2} \right], \quad (4)$$

288 where $G_{\rightarrow(3)}^{\circ}$ is the free energy of reaction (3) and it is assumed that tugarinovite is pure MoO₂
289 (the small grain size of tugarinovite makes it impossible to assess purity based on the analysis
290 given in Table 2). Taking the free energy of formation of MoO₂ from the JANAF tables (Chase
291 et al. 1985), leads to calculated activity coefficients of 0.06 (500°C) - 0.20 (800°C), which reflect
292 negative deviations from ideality, consistent with available thermodynamic data (e.g.,
293 Kleykamp 1989; Mazhuga et al. 1998). Thus, we cannot distinguish on this basis whether the
294 Ru-Mo-Ni alloy is a relict high temperature phase that did not equilibrate with MoO₂ or it is an
295 alteration phase that did equilibrate with tugarinovite.

296 Nickel, Fe, V, Mo, and P are generally viewed as being mobile during the alteration of
297 Allende CAIs (e.g., Campbell et al. 2003; Paque et al. 2007) so that the current Mo/P of the
298 monipite-bearing opaque assemblage, in particular, is probably not the same as it was prior to
299 alteration. This makes specific identification of possible precursor phases difficult to establish
300 based on major element chemistry. However, the observation of multiple occurrences of apatite,
301 kamiokite and tugarinovite in the host CAI, suggests that these phases represent important
302 pathways by which metamorphism of Mo-, P-enriched precursors within this CAI was expressed.
303 Campbell et al. (2003), for example, argued based on the PGE signature that schreibersite was
304 originally present in the precursor to an opaque assemblage they studied in Allende but that the
305 schreibersite was destroyed during metasomatism. In the present opaque inclusion, Mo and P
306 concentrations in the precursor were much higher, so that monipite rather than schreibersite was

307 the dominant phosphide and Mo concentrations were sufficiently high to support the formation
308 of large amounts of Mo oxides.

309 Armstrong et al. (1985) and Bischoff and Palme (1987) described opaque assemblages
310 from Allende CAIs that contain Mo-rich areas but these differ from the objects of this study in
311 three important respects. First, Mo is in the form of powellite-scheelite (i.e., Ca molybdate-
312 tungstate) rather than the Fe-Mo oxides tugarinovite and kamiokite; second, apatite is rare or
313 absent; and, third, no phosphides are observed. These three observations are not unrelated. In
314 the presence of large amounts of phosphide, incoming Ca vapors, probably mostly in the form of
315 Ca(OH)_2 (Hashimoto 1992), reacted with P in Fe-Ni alloys and phosphides to form apatite. For
316 monipite the overall reaction would have been



318 for the hydrated form of apatite and a similar reaction can be written for chloride transport. In
319 the absence of significant amounts of phosphides, as is more typical of opaque assemblages
320 (Armstrong et al. 1985; Bischoff and Palme 1987), a Ca molybdate forms in preference to the
321 oxides tugarinovite and kamiokite. Note in Eqn. (5), that the molar Mo/P ratio of the product
322 apatite + tugarinovite is 1 because the monipite source has a fixed ratio. Based on modes within
323 the opaque assemblage shown in Fig. 1b, the molar Mo/P ratio would be approximately 2. This
324 suggests that either P was preferentially lost from the opaque assemblage relative to Mo or,
325 perhaps more likely, that there was more Mo than P in the precursor (i.e., the precursor consisted
326 of monipite and additional Mo-bearing phases, probably in the form of alloys).

327 The above considerations suggest the following basic scenario for the formation of
328 monipite. The host CAI is the product of melting to temperatures on the order of 1400°C,
329 followed by cooling at degrees to tens of degrees per hour. During this melting event, Mo, P, Fe,
330 and Ni formed immiscible metallic melts within the silicate melt of the host. During cooling,
331 either monipite crystallized from the metallic melt (or a P-rich immiscible melt within the alloy
332 melt), or it exsolved at lower temperatures from a Mo-P enriched crystalline alloy. At a later
333 time, the host CAI was subjected to an alteration event that oxidized Mo and P to form apatite
334 and Mo oxides. There are currently insufficient thermodynamic, kinetic, and phase equilibria
335 data involving monipite to quantify the history of this phase but, if available, they could, in
336 principle, be used to help constrain several important facets of CAI evolution including the

337 nature of the melting event and of siderophile precursor materials and the evolution of Mo and P
338 in CAIs both during the melting event and during later alteration.

339

340

ACKNOWLEDGEMENTS

341 The Caltech GPS Analytical Facility is supported, in part, by NSF grants NSF EAR-
342 0318518 and DMR-0080065. We also acknowledge NASA grant NNG04GG14G and NSF
343 grant EAR-0947956. We thank Alan Rubin, an anonymous reviewer and associate editor Oliver
344 Tschauner for helpful reviews.

345

346

REFERENCES CITED

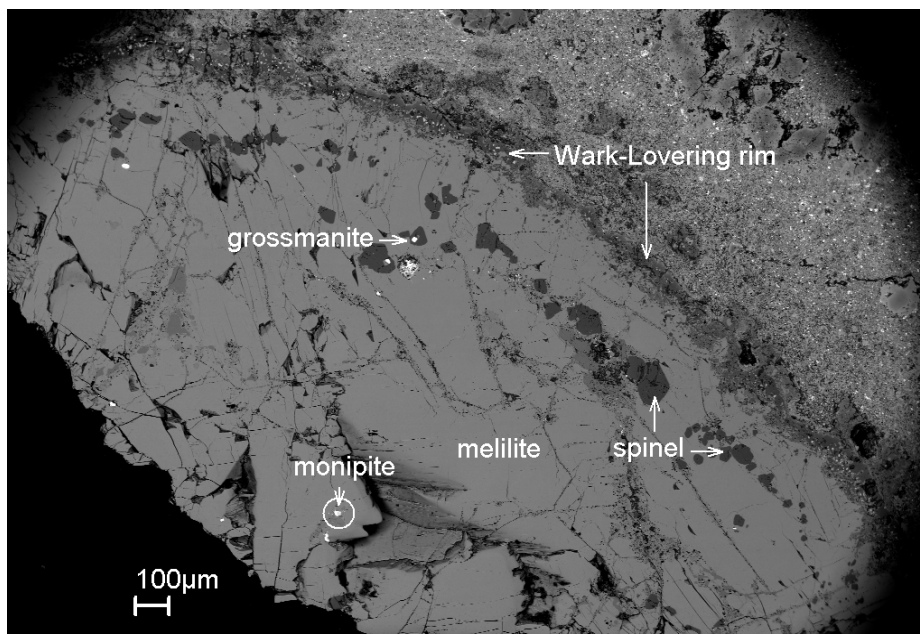
- 347 Armstrong, J.T., El Goresy, A., and Wasserburg, G.J. (1985) Willy: A prize noble Ur-
348 Fremdling—Its history and implications for the formation of Fremdlinge and CAI.
349 *Geochimica et Cosmochimica Acta*, 49, 1001-1022.
- 350 Armstrong, J.T., Hutcheon, I.D., and Wasserburg, G.J. (1987) Zelda and company: Petrogenesis
351 of sulfide-rich Fremdlinge and constraints on solar nebula processes. *Geochimica et*
352 *Cosmochimica Acta*, 51, 3155-3173.
- 353 Armstrong, J.T. (1995) CITZAF: A package of correction programs for the quantitative electron
354 beam X-ray analysis of thick polished materials, thin films, and particles. *Microbeam*
355 *Analysis*, 4, 177-200.
- 356 Bischoff, A. and Palme, H. (1987) Composition and mineralogy of refractory-metal-rich
357 assemblages from a Ca,Al-rich inclusion in the Allende meteorite. *Geochimica et*
358 *Cosmochimica Acta*, 51, 2733-2748.
- 359 Blum, J.D., Wasserburg, G.J., Hutcheon, I.D., Beckett, J.R., and Stolper, E.M. (1989) Origin of
360 opaque assemblages in C3V meteorites: Implications for nebular and planetary processes.
361 *Geochimica et Cosmochimica Acta*, 53, 543-556.
- 362 Campbell, A.J., Simon, S.B., Humayun, M., and Grossman, L. (2003) Chemical evolution of
363 metal in refractory inclusions in CV3 chondrites. *Geochimica et Cosmochimica Acta*, 67,
364 3119-3134.
- 365 Chase, M.W., Davies, C.A., Downey, J.R., Frurip, D.J., McDonald, R.A., and Syverud, A.N.
366 (1985) JANAF thermochemical tables third edition. Physical and Chemical Reference
367 data, 14, Supplement 1, 1-1856.

- 368 Chuang, Y.-Y., Chang, Y.A., Schmid, R., and Lin, J.-C. (1986) Magnetic contributions to the
369 thermodynamic functions of alloys and the phase equilibria of the Fe-Ni system below
370 1200 K. *Metallurgical Transactions*, 17A, 1361-1372.
- 371 Gabriel, A., Gustafson, P., and Ansara, I. (1987) A thermodynamic evaluation of the C-Fe-Ni
372 system. *Calphad*, 11, 203-218.
- 373 Grossman, L., Simon, S.B., Rai, V.K., Thiemens, M.H., Hutcheon, I.D., Williams, R.W., Galy,
374 A., Ding, T., Fedkin, A.V., Clayton, R.N., and Mayeda, T.K. (2008a) Primordial
375 compositions of refractory inclusions. *Geochimica et Cosmochimica Acta*, 72, 3001-
376 3021.
- 377 Grossman, L., Beckett, J.R., Fedkin, A.V., Simon, S.B., and Ciesla, F.J. (2008b) Redox
378 conditions in the solar nebula: Observational, experimental, and theoretical constraints.
379 *Reviews in Mineralogy & Geochemistry*, 68, 93-140.
- 380 Guérin, P.R. and Sergent, M. (1977) Structure Cristalline de NiMoP. *Acta Crystallographica*,
381 B33, 2820-2823.
- 382 Hashimoto, A. (1992) The effect of H₂O gas on volatilities of planet-forming major elements: I.
383 Experimental determination of thermodynamic properties of Ca-, Al-, and Si-hydroxide
384 gas molecules and its application to the solar nebula. *Geochimica et Cosmochimica*
385 *Acta*, 56, 511-532.
- 386 Jambor, J.L., Kovalenker, V.A., and Roberts, A.C. (2000) New mineral names. *American*
387 *Mineralogist*, 85, 873-877.
- 388 Kleykamp, H. (1989) Constitution and thermodynamics of the Mo-Ru, Mo-Pd, Ru-Pd, and Mo-
389 Ru-Pd systems. *Journal of Nuclear Materials*, 167, 49-63.
- 390 Koyama, K., Morishita, M., Harada, T., and Maekawa, N. (2003) Determination of standard
391 Gibbs energies of formation of Fe₂Mo₃O₁₂, Fe₂Mo₃O₈, Fe₂MoO₄, and FeMoO₄ of the Fe-
392 Mo-O ternary system and μ phase of the Fe-Mo binary system by electromotive force
393 measurement using a Y₂O₃-stabilized ZrO₂ solid electrolyte. *Metallurgical and Materials*
394 *Transactions*, 34B, 653-659.
- 395 Lovering, J.F., Wark, D.A., and Sewell, D.K.B. (1979) Refractory oxide, titanite, niobate and
396 silicate accessory mineralogy of some type B Ca-Al-rich inclusions in the Allende
397 meteorite. *Lunar and Planetary Science*, 10, 745-747.

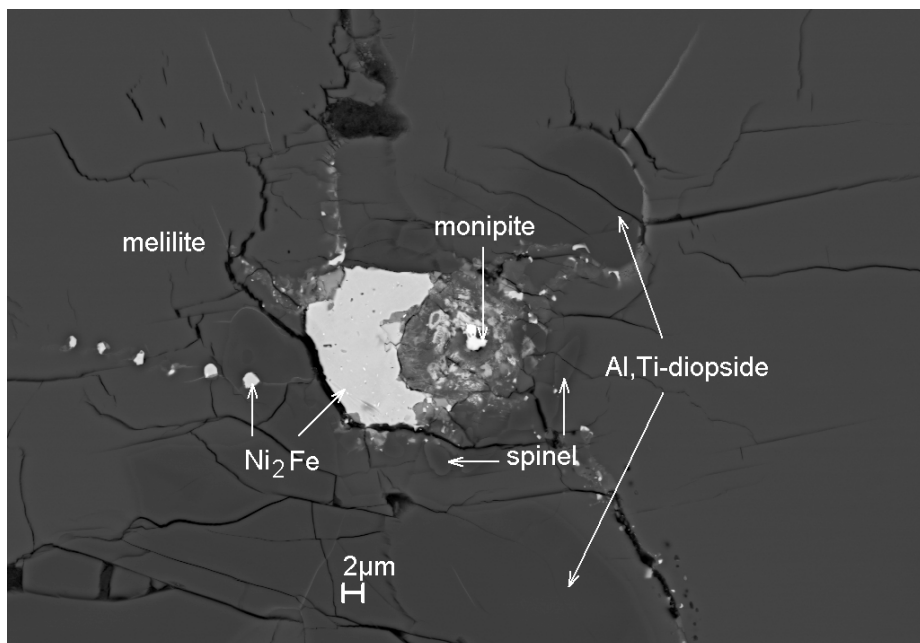
- 398 Ma, C. and Inoue, A. (2003) Microstructure and mechanical properties of Cr, Mo, Fe, Ta
399 modified Pd-Ni-Cu-P glassy alloys prepared by copper-mold casting. *Materials*
400 *Transactions*, 44, 188-196.
- 401 Ma, C. and Rossman, G.R. (2008) Barioperovskite, BaTiO₃, a new mineral from the Benitoite
402 Mine, California. *American Mineralogist*, 93, 154-157.
- 403 Ma, C. and Rossman, G.R. (2009a) Tistarite, Ti₂O₃, a new refractory mineral from the Allende
404 meteorite. *American Mineralogist*, 94, 841-844.
- 405 Ma, C. and Rossman, G.R. (2009b) Grossmanite, CaTi³⁺AlSiO₆, a new pyroxene from the
406 Allende meteorite. *American Mineralogist*, 94, 1491-1494.
- 407 Ma, C., Beckett, J.R., and Rossman, G.R. (2009a) Discovery of a new phosphide mineral,
408 monipite (MoNiP), in an Allende type B1 CAI. *Meteoritics & Planetary Science*, 44,
409 A127.
- 410 Ma, C., Beckett, J.R., and Rossman, G.R. (2009b) Allendeite and hexamolybdenum: two new
411 ultra-refractory minerals in Allende and two missing links. *Lunar and Planetary Science*
412 *Conference 40*, Abstract #1402.
- 413 Ma, C. (2010) Hibonite-(Fe), (Fe,Mg)Al₁₂O₁₉, a new alteration mineral from the Allende
414 meteorite. *American Mineralogist*, 95, 188-191.
- 415 Mazhuga, T.G., Danilenko, V.M., Velikanova, T.Ya., and Semenova, E.L. (1998)
416 Thermodynamic calculation of phase equilibria in the Ti-Ru, Ti-Os, Ni-Ru binary
417 systems. *Calphad*, 22, 59-67.
- 418 McMahan, B.M. and Haggerty, S.E. (1980) Experimental studies bearing on the magnetite-alloy-
419 sulfide association in the Allende meteorite: Constraints on the conditions of chondrule
420 formation. *Proceedings of the Lunar and Planetary Science Conference*, 11, 1003-1025.
- 421 Mendybaev, R.A., Richter, F.M., and Davis, A.M. (2006) Crystallization of melilite from
422 CMAS-liquids and the formation of the melilite mantle of Type B1 CAIs: Experimental
423 simulations. *Geochimica et Cosmochimica Acta*, 70, 2622-2642.
- 424 Nagai, M., Fukiage, T., and Kurata, S. (2005) Hydrodesulfurization of dibenzothiophene over
425 alumina-supported nickel molybdenum phosphide catalysts. *Catalysis Today*, 106, 201-
426 205.
- 427 O'Neill, H.St.C. (1986) Mo-MoO₂ (MOM) oxygen buffer and the free energy of formation of
428 MoO₂. *American Mineralogist*, 71, 1007-1010.

- 429 Oryshchyn, S.V., Le Sénéchal, C., Députier, S., Bauer, J., Guérin, R., and Akselrud, L.G. (2001)
430 New ternary phases in the Mo-Ni-P system: Synthesis and crystal structures. *Journal of*
431 *Solid State Chemistry*, 160, 156-166.
- 432 Paque, J.M., Burnett, D.S., and Beckett, J.R. (2007) Zoning patterns of Fe and V in spinel from a
433 type B Ca-Al-rich inclusion: Constraints on subsolidus thermal history. *Meteoritics &*
434 *Planetary Science*, 42, 899-912.
- 435 Pouchou, J.-L. and Pichoir, F. (1991) Quantitative analysis of homogeneous or stratified
436 microvolumes applying the model "PAP". In *Electron Probe Quantitation* (Heinrich,
437 K.F.J. and Newbury, D.E., eds.), Plenum Press, 31-75.
- 438 Riches, A.J.V., Liu, Y., Zhang, A., and Taylor, L.A. (2010) Description of newly-identified CV3
439 chondrites: Salient textural and mineralogical characteristics. *Lunar and Planetary*
440 *Science* 41, Abstract #2561.
- 441 Richter, F.M., Davis, A.M., Ebel, D.S., and Hashimoto, A. (2002) Elemental and isotopic
442 fractionation of Type B calcium-, aluminum-rich inclusions: Experiments, theoretical
443 considerations, and constraints on their evolution. *Geochimica et Cosmochimica Acta*,
444 66, 521-540.
- 445 Shirotni, I., Takaya, M., Kaneko, I., Sekine, C., and Yagi, T. (2000) Superconductivity of
446 MRuP and MNiP (M = Mo or W) prepared at high pressure. *Solid State*
447 *Communications*, 116, 683-686.
- 448 Simon, S.B., Davis, A.M., and Grossman, L. (1999) Origin of compact type A refractory
449 inclusions from CV3 carbonaceous chondrites. *Geochimica et Cosmochimica Acta*, 63,
450 1233-1248.
- 451 Stolper, E. (1982) Crystallization sequences of Ca-Al-rich inclusions from Allende: An
452 experimental study. *Geochimica et Cosmochimica Acta*, 46, 2159-2180.
- 453 Stolper, E. and Paque, J.M. (1986) Crystallization sequences of Ca-Al-rich inclusions from
454 Allende: The effects of cooling rate and maximum temperature. *Geochimica et*
455 *Cosmochimica Acta*, 50, 1785-1806.
- 456 Stolper, E., Paque, J., and Rossman, G.R. (1982) The influence of oxygen fugacity and cooling
457 rate on the crystallization of Ca-Al-rich inclusions from Allende. *Lunar and Planetary*
458 *Science* 13, 772-773.

- 459 Sun, F., Wu, W., Wu, Z., Wei, Z., Yang, Y., Jiang, Z., Tian, F., and Li, C. (2004)
460 Dibenzothiophene hydrosulfurization activity and surface sites of silica-supported MoP,
461 Ni₂P, and Ni-Mo-P catalysts. *Journal of Catalysis*, 228, 298-310.
- 462 Vogel, R. and Horstmann, D. (1953) Das Zustandsschaubild Eisen-Eisenphosphid-
463 Molybdänphosphid-Molybdän. *Archiv für das Eisenhüttenwesen*, 24, 369-374.
- 464 Waldner, P. and Pelton, A.D. (2004) Critical thermodynamic assessment and modeling of the Fe-
465 Ni-S system. *Metallurgical and Materials Transactions*, 35B, 897-907.
- 466 Wark, D.A. and Boynton, W.V. (2001) The formation of rims on calcium-aluminum-rich
467 inclusions: Step I—Flash heating. *Meteoritics & Planetary Science*, 36, 1135-1166.
468
469

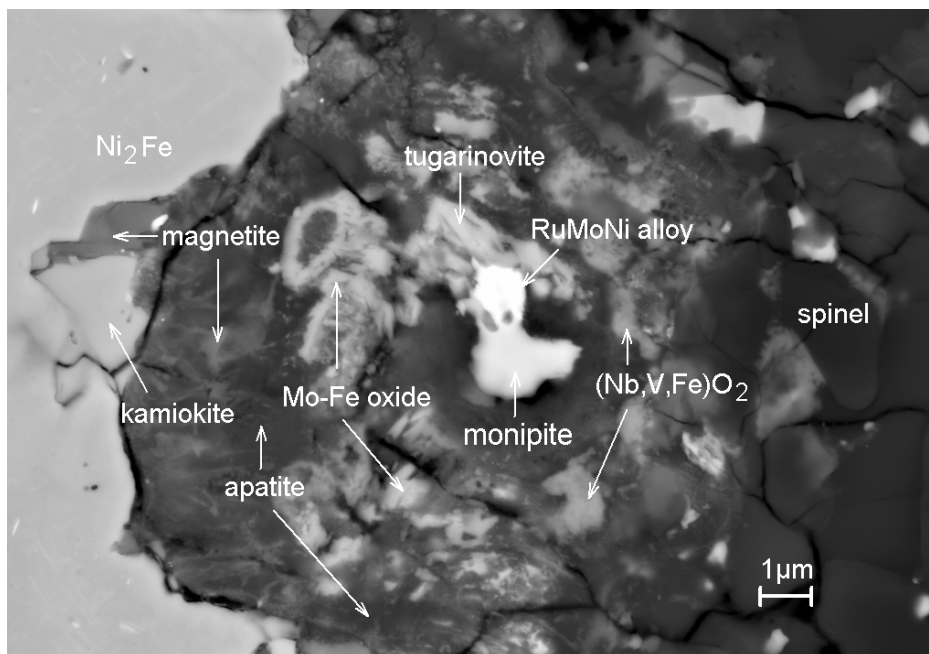


470
471 Figure 1a. Backscatter electron (BSE) image of CAI host of the monipite-bearing phase
472 assemblage in USNM 7554. The location of monipite is enclosed by a circle.
473



474
475 Figure 1b. BSE image showing the region where the monipite micro-crystal and its associated
476 phases are located. The opaque assemblage is bounded on one side mostly by Al,Ti-diopside
477 and spinel and on the other mostly by melilite.
478

479



480

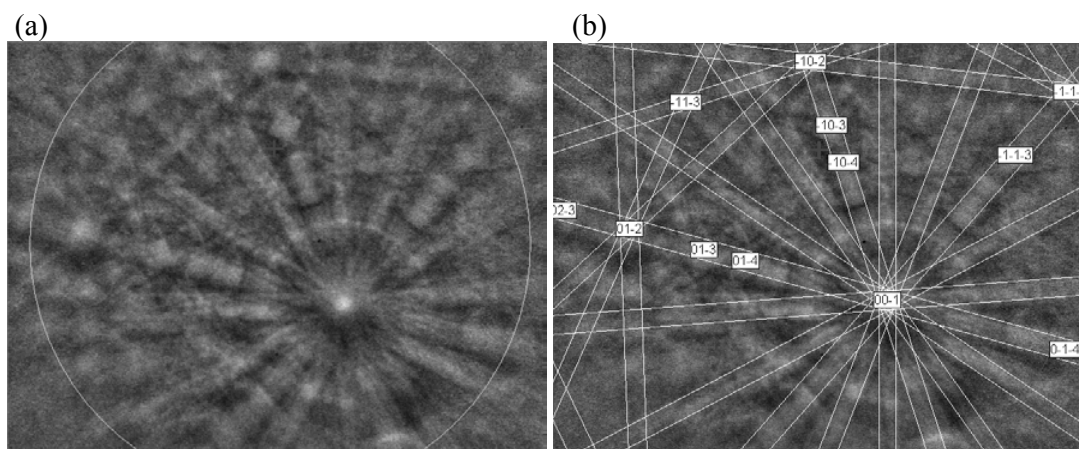
481

482 Figure 2. Enlarged BSE image showing the monipite micro-crystal and its associated phases.

483

484

485

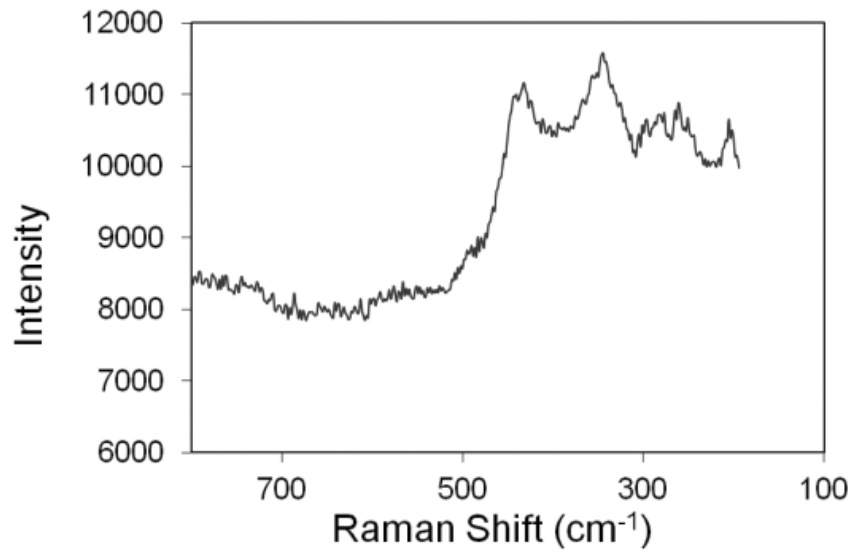


486

487

488 Figure 3. (a) EBSD pattern of the monipite crystal, (b) Pattern indexed using the MoNiP $P\bar{6}2m$
489 structure of Guérin and Sergent (1977).

490
491
492

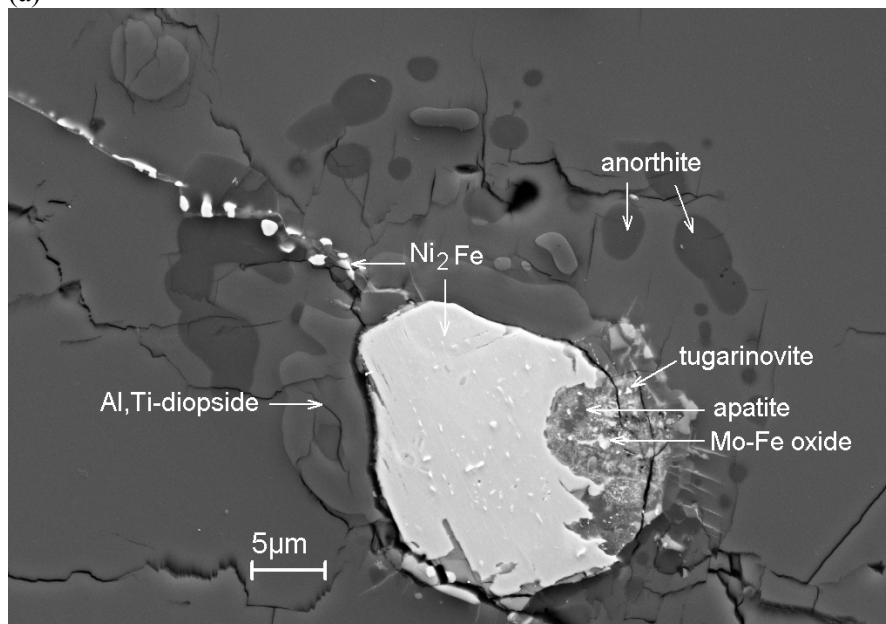


493
494
495
496

Figure 4. Raman spectrum of type monipite.

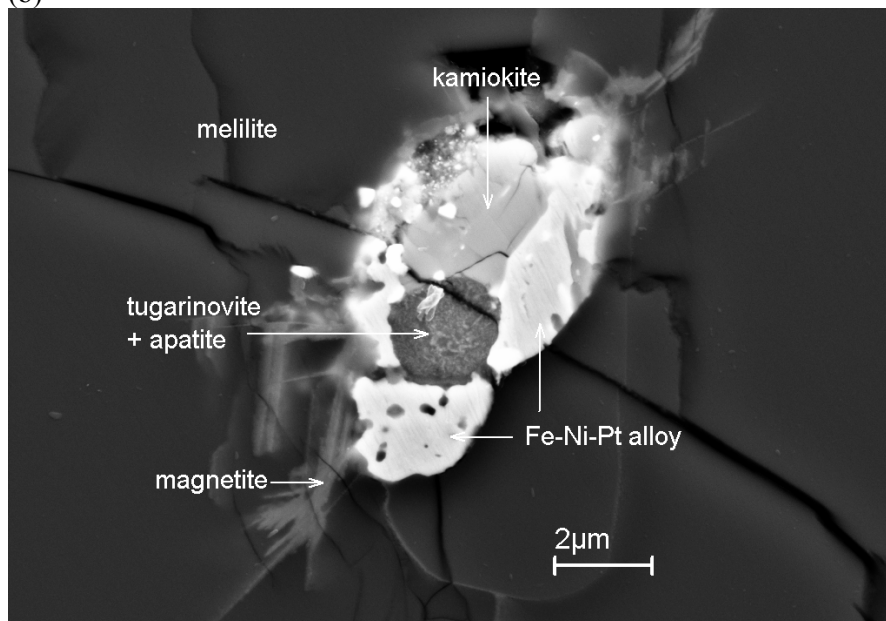
497
498

(a)



499
500

(b)



501
502
503
504
505
506

Figure 5. Phosphate - Mo oxide - magnetite - awaruite assemblages. (a) The opaque assemblage is partially enclosed by Al,Ti-diopside with a surrounding rosette of anorthite blebs, the latter most likely reflecting trapped melt. Ni-Fe alloy are scattered along a crack that extends from the opaque assemblage. (b) Phosphate - tugarinovite region surrounded by Pt-bearing Fe-Ni alloy and kamiokite.

Table 1: Oxides, phosphates, and silicates within and around or near the monipite-bearing phase assemblage

Phase	Al,Ti-diopside	melilite	spinel	kamiokite	V-rich magnetite	(Nb,V,Fe)O ₂ ^a	apatite ^b	Tugarinovite ^c	Mo-Fe-oxide ^d
Section	USNM 7554	USNM 7554	USNM 7554	USNM 7554	USNM 7554	USNM 7554	USNM 7554	USNM 7554	USNM 7554
type	EPMA ^e	EPMA	SEM-EDS ^f	SEM-EDS	SEM-EDS	SEM-EDS	SEM-EDS	SEM-EDS	SEM-EDS
# analyses	7	6	1	1	1	1	1	1	1
Na ₂ O	0.01 (0.01)	0.02 (0.01)	n.d.	n.d.	n.d.	n.d.	n.d.	n.d.	n.d.
MgO	8.0 (0.6) ^e	2.84 (0.03)	17.4 (0.3) ^f	2.5 (0.1)	1.1 (0.1)	1.2 (0.2)	1.9 (0.2)	0.9 (0.3)	0.8 (0.3)
Al ₂ O ₃	20.5 (0.9)	29.4 (0.1)	63.7 (0.6)	n.d.	3.0 (0.2)	1.2 (0.2)	n.d.	n.d.	n.d.
SiO ₂	38 (1)	26.5 (0.1)	n.d.	n.d.	1.1 (0.2)	n.d.	n.d.	n.d.	n.d.
P ₂ O ₅	n.d. ^g	n.d.	n.d.	n.d.	n.d.	11.6 (0.6)	41.9 (0.9)	3.1 (0.6)	22 (1)
CaO	25.5 (0.2)	41.9 (0.2)	n.d.	0.81 (0.1)	1.7 (0.1)	20.0 (0.5)	47.8 (0.8)	4.1 (0.4)	28.8 (0.9)
TiO ₂	7 (1)	0.01 (0.01)	n.d.	n.d.	n.d.	n.d.	n.d.	n.d.	n.d.
V ₂ O ₃	0.7 (0.3)	0.01 (0.01)	2.6 (0.2)	n.d.	13.4 (0.3)	13.1 (0.6)	n.d.	n.d.	n.d.
Cr ₂ O ₃	0.10 (0.03)	n.d.	n.d.	n.d.	1.2 (0.2)	n.d.	n.d.	n.d.	n.d.
MnO	0.01 (0.01)	n.d.	n.d.	n.d.	n.d.	n.d.	n.d.	n.d.	n.d.
FeO ^h	0.09 (0.01)	0.05 (0.04)	16.3 (0.5)	21.7 (0.4)	71.4 (0.5)	6.7 (0.5)	0.6 (0.7)	6.8 (0.8)	14 (1)
NiO	0.08 (0.02)	0.03 (0.03)	n.d.	1.0 (0.3)	n.d.	n.d.	n.d.	n.d.	n.d.
Nb ₂ O ₅	n.d.	n.d.	n.d.	n.d.	n.d.	46 (1)	n.d.	n.d.	n.d.
MoO ₂	n.d.	n.d.	n.d.	74.0 (0.6)	7.2 (0.4)	n.d.	7.9 (0.9)	85 (1)	34 (1)
Total	99.99	100.76	100.0	100.0	100.1	99.8	100.1	99.9	99.6
# Oxygens	6 ^f	7	4	8	4 ^f				
Na	n.d.	0.00	n.d.	n.d.	n.d.				
Mg	0.45	0.19	0.67	0.32	0.06				
Al	0.90	1.57	1.93	n.d.	0.12				
Si	1.42	1.20	n.d.	n.d.	0.04				
P	n.d.	n.d.	n.d.	0.00	n.d.				
Ca	1.02	2.03	n.d.	0.07	0.06				
Ti	-	0.00	n.d.	n.d.	n.d.				
Ti ³⁺	0.05	-	-	-	-				
Ti ⁴⁺	0.14	-	-	-	-				
V	0.02	0.00	0.05	n.d.	0.39				
Cr	0.00	0.00	n.d.	n.d.	0.03				
Mn	0.00	0.00	n.d.	n.d.	n.d.				
Fe*	0.00	0.00	-	1.56	-				
Fe ²⁺	-	-	0.35	-	1.06				
Fe ³⁺	-	-	-	-	1.11				
Ni	0.00	n.d.	n.d.	0.07	n.d.				
Zr	n.d.	n.d.	n.d.	n.d.	n.d.				
Mo	n.d.	n.d.	n.d.	2.99	0.12				
Sum cations	4.00	5.01	3.00	5.01	3.00				

^aAnalysis contaminated by apatite.

^bAnalysis contaminated by tugarinovite.

^cAnalysis contaminated by apatite, Mo-Fe-oxide.

^dAnalysis contaminated by apatite and tugarinovite. This phase has a cubic structure, based on EBSD.

^eErrors given inside parentheses for EPMA analyses are one standard deviation of the mean based on all of the analyses.

^fErrors given inside parentheses for SEM-EDS analyses are one standard deviation computed from counting statistics.

^gn.d.: not determined.

^hAll Fe as FeO.

ⁱFormula computed assuming exactly 4.00 cations in a formula unit based on 6.00 oxygens by adjusting cations of Ti^{3+} and Ti^{4+} .

^jFormula computed assuming exactly 3.00 cations in a formula unit based on 4.00 oxygens by adjusting cations of Fe^{2+} and Fe^{3+} .

Table 2: Alloys and Phosphides in Monipite-bearing Phase Assemblages

Phase	monipite	Ru-Mo-Ni alloy	Ni ₂ Fe alloy
Section	USNM 7554	USNM 7554	USNM 7554
type	EPMA ^a	SEM-EDS ^b	SEM-EDS
# analyses	3	1	1
P	16.8 (0.2) ^a	n.d.	n.d.
Fe	1.73 (0.07)	n.d.	32.8 (0.8)
Co	1.25 (0.05)	n.d.	n.d.
Ni	28.5 (0.2)	14.1 (0.8) ^b	65.9 (0.9)
Mo	43.9 (0.6)	29 (1)	n.d.
Ru	5.2 (0.1)	53 (1)	n.d.
Rh	1.93 (0.07)	4(1)	n.d.
Pt	n.d. ^c	n.d.	1.3 (0.7)
Total	99.31	100.1	100.0
	Based on 1 P	Atomic %	Atomic %
P	1		
Fe	0.06	n.d.	34.23
Co	0.04	n.d.	n.d.
Ni	0.89	21.67	65.39
Mo	0.84	27.67	n.d.
Ru	0.09	47.13	n.d.
Rh	0.03	3.53	n.d.
Pt	n.d.	n.d.	0.38
Sum	2.96	100.00	100.00

^aErrors given inside parentheses for EPMA analyses are one standard deviation of the mean based on all of the analyses.

^bErrors given inside parentheses for SEM-EDS analyses are one standard deviation computed from counting statistics.

^cn.d.: not determined.